Photothermal self-stability and optical bistability of single NaCl–water microdroplets on a superhydrophobic surface

Y. Karadag, M. Mestre and A. Kiraz*

Received 23rd February 2009, Accepted 14th May 2009
First published as an Advance Article on the web 10th June 2009
DOI: 10.1039/b903800k

A self-stabilization mechanism locking the size of single inorganic salt (NaCl)–water microdroplets that are standing on a superhydrophobic surface and kept in a humidity-controlled chamber is demonstrated. The effect is based on the hysteretic behavior of a photothermal tuning cycle caused by the whispering gallery mode (WGM) absorption resonances that are observed when scanning the power of an infrared laser focused at the rim of a microdroplet. When locked, the microdroplet size and WGM spectrum are resilient to environmental perturbations and can be maintained for hours as the mechanism does not rely on a photobleachable dye. The bistable nature of the system is also demonstrated, enabling reversible switching between two sizes. A rate equation-based thermodynamical model of the hysteretic behavior is provided, giving good agreement with the experimental results. Our results may be used to establish stable experimental conditions for ultrahigh resolution spectroscopy of microdroplets. Other optical and biological applications that require exactly size-matched microdroplets can also benefit from the demonstrated self-stabilization mechanism.

I. Introduction

Ensuring stable experimental conditions is essential in ultra-high resolution characterization of an ultrahigh quality optical microcavity.[1] This becomes an especially critical challenge in the study of liquid microdroplets which confine ultrahigh quality whispering gallery modes (WGMs), owing to their spherical shape and smooth surface.[2,3] Because of their flexible nature, WGMs of liquid microdroplets can be easily tuned using evaporation/condensation[4] or simple geometrical deformation.[5] On one hand, large spectral tunability is an important advantage of liquid microdroplets over other solid optical microcavities that can prove to be important in various applications such as designing tunable light sources or optical communications devices. On the other hand it shows the fragility of the system, and, hence, may prevent ultrahigh resolution characterization of the WGMs.

Adding a non-volatile component such as glycerol[6] or an inorganic salt[7] to water microdroplets, and keeping them in a chamber with a fixed relative water humidity are commonly-used first steps in stabilizing the experimental conditions while studying liquid microdroplets. However, unless an active stablization loop is implemented, these are not sufficient for long time stabilization of microdroplets, especially at high relative water humidities where the microdroplet becomes very sensitive to changes in the ambient atmosphere.[3] Here, we demonstrate a self-stabilization mechanism that stabilizes the size of individual NaCl–water microdroplets over long time periods. We also explain the mechanism based on the model of photothermal tuning that we have recently developed.[6,7] In contrast to our previous demonstrations where the microdroplet was locally heated by an infrared laser focused at its center,[6,7] in this study the infrared laser's focus is positioned near the microdroplet's rim. This gives rise to the observation of high quality WGM resonances in the infrared laser absorption which lead to a hysteretic behavior in a photothermal tuning cycle where the infrared laser power is first increased and then decreased. Hysteresis curves reveal operation points where the volume of a microdroplet can be self-stabilized for long time periods. We further study the optical bistability[8] obtained from the hysteresis curves and demonstrate a microdroplet-based optical memory device operating by almost reversibly changing the size of a microdroplet between two values at a given infrared laser power.

Optical bistability was previously observed in electro-dynamically-trapped liquid microdroplets.[9,10] Those experiments relied on the excitation of dye-doped microdroplets with a tunable laser. Hysteresis loops were observed in the light-scattering measurements performed as the tunable laser wavelength was scanned. Observed bistability was explained by evaporation or condensation of the microdroplet due to dye absorption. We have also recently demonstrated self-stability in dye-doped water microdroplets standing on a superhydrophobic surface.[11] In our demonstration, self-stability relied on the evaporation or condensation due to dye absorption of a green laser. Photobleaching prevented the demonstration of long time stability in those experiments (maximum stabilization time was $\sim$2 min). In contrast to the previous works on optical bistability and self-stability of liquid micro-droplets, the experiments reported in this work rely on the infrared laser absorption of the water molecules, which is not affected by photobleaching. As a result, we demonstrate photothermal self-stabilization for several hours. In addition,

Department of Physics, Koç University, Rumelifeneri Yolu, Sariyer, 34450 Istanbul, Turkey. E-mail: akiraz@ku.edu.tr

in this article we fully model the evaporation/condensation dynamics of the liquid microdroplet as a result of infrared laser absorption using a rate equation-based thermodynamical model.

For solid optical microcavities, thermal self-stability was previously demonstrated in microtoroids.[1] In that system, the self-stabilization mechanism relied on the expansion and refractive index change of the microcavity as a result of laser heating.

This article is organized as follows. In section 2, the theoretical model based on the lumped system formulation of mass and energy conservations is explained, and an exemplary calculation of absorption of an infrared laser focused near the rim of a microdroplet is made. Hysteretic behavior in a photothermal tuning cycle is then predicted by considering the theoretical model and calculated infrared laser absorption. The sample preparation and experimental setup are described in section 3. The experimental results are presented in section 4. These include the demonstrations of the hysteretic behavior, resilience to an external perturbation, long time self-stabilization, and optical bistability. Conclusions are discussed in section 5.

II. Theory

A Model used for photothermal tuning

Lumped system formulation of mass and energy conservations is used to model photothermal tuning. This model assumes that all the variables of the microdroplet and the chamber are uniform throughout their whole respective volumes, as described previously.[6,7] According to the model, the rate of change of the number of moles of water (N_A) in the microdroplet depends on the relative water humidity in the chamber (S_A) and the water vapor pressure at the surface of the droplet (governed by the activity coefficient γ_A determined by the amount of salt) via:

$$\frac{dN_A}{dt} = -4\pi a f_{PB} D_A \frac{P_A^0(T_\infty)}{RT_\infty}(\gamma_A x_A \phi_A - S_A). \quad (1)$$

The temperature change in the microdroplet is due to the evaporation of water, conductive heat loss, and photothermal heating, and is given as:

$$\frac{dT_d}{dt} = \frac{\Delta H_{vap,A}}{NC_{PL}}\frac{dN_A}{dt} - \frac{3k_{eff}V_m}{a^2 C_{PL}}(T_d - T_\infty) + \frac{\tilde{Q}_{abs}P_{inc}}{NC_{PL}}, \quad (2)$$

where

$$\phi_A = \left(\frac{T_\infty}{T_d}\right)\frac{P_A^0(T_d)}{P_A^0(T_\infty)}. \quad (3)$$

In eqn (1)–(3), D_A is the molecular diffusivity in the gas mixture, x_A is the mole fraction of water, R is the universal gas constant, $P_A^0(T)$ is the vapor pressure at temperature T, and T_d and T_∞ are the temperatures at the air–microdroplet interface and in the chamber far from the microdroplet, V_m is the molar specific volume, C_{PL} is the molar heat capacity of the microdroplet mixture, k_{eff} is the area average of the heat conductivities of the air and the substrate,[7] and $\tilde{Q}_{abs}$ is the ratio of the total power absorbed by the droplet to the total power of the incident beam (P_{inc}) respectively. The correction factor, f_{PB}, is calculated by using the Picknett and Bexon[12,13] equation assuming a typical contact angle of $\theta = 160°$. The water activity coefficient (γ_A) and solution density (ρ) in g cm^{-3} of NaCl–water microdroplets are computed using the polynomial best fit coefficients given in ref. 14. In the simulations, C_{PL} is also dynamically calculated as a function of the salt concentration.[15]

B Hysteresis behavior

Fig. 1a shows the result of the $\tilde{Q}_{abs}$ calculation as a function of the size parameter $\alpha = 2\pi a/\lambda$, where a and λ are the radius of the microdroplet and wavelength, respectively. This calculation was performed using the localized approximation to the beam-shape coefficients in generalized Lorenz–Mie theory[16,17] with an improved algorithm.[18] In our experimental conditions, the NaCl concentration in microdroplets is 3.83 M at

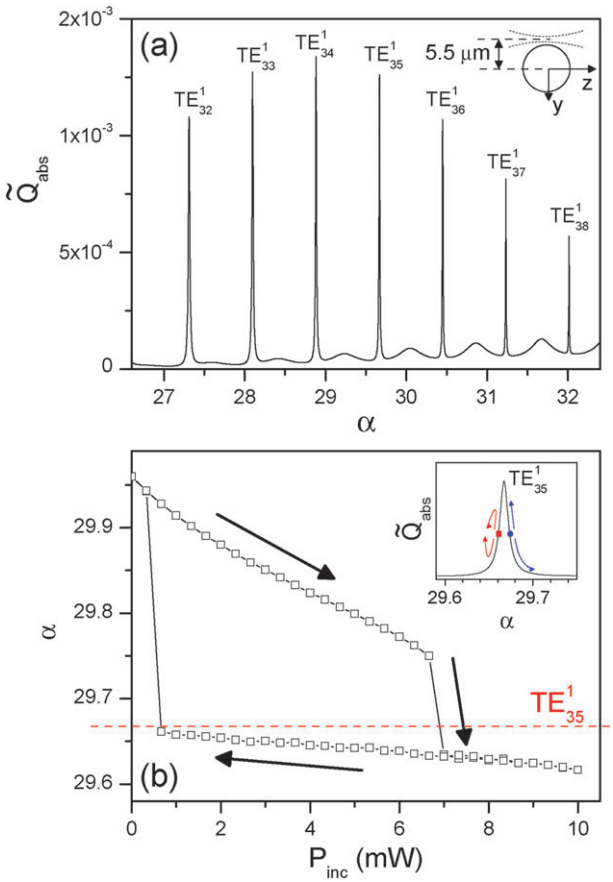

Fig. 1 (a) The modified absorption efficiency ($\tilde{Q}_{abs}$) of a focused Gaussian beam as a function of the size parameter (α). The beam propagating along z and polarized along x directions is focused near the rim of the sphere at $y = 5.5$ μm, exciting first order TE modes. (b) The computed hysteresis curve as a function of the incident laser power. The dashed horizontal line shows the peak position of the TE^1_{35} WGM absorption. Inset shows the sketch of the self-stabilization mechanism.

equilibrium. Hence, the refractive index of the microdroplet was assumed to be $n = 1.3544 + 1112.15 \times 10^{-9}i$ in this calculation. The real part of the refractive index was determined by converting the value for a 3.83 M NaCl–water solution at 589 nm[19] to 1064 nm.[20] The absorption coefficient of pure water at 1064 nm[21] was converted to that of a 3.83 M NaCl–water solution[14] in determining the imaginary part of the refractive index. A Gaussian beam with a focal waist of $w_0 = 1000$ nm that is propagating along z and linearly polarized along x directions was considered to be focused 5.5 μm away from the microdroplet's center along the y direction, as shown in the inset in Fig. 1a. The angular momentum number and radial mode order of the high quality WGMs are shown in Fig. 1a. Only TE WGMs are excited due to the selected focal point and polarization.[2]

In Fig. 1b we show the change in α as P_{inc} is first gradually increased from 0 to 10 mW, and then decreased back to 0 mW, computed using the $\tilde{Q}_{abs}$ function shown in Fig. 1a. In this calculation, the initial size parameter ($\alpha = 29.96$ corresponding to $a = 5.0735$ μm) is intentionally selected to be slightly larger than the position of the TE_{35}^{1} WGM absorption that peaks at $\alpha = 29.67$. Hysteretic behavior is clearly observed in the calculated photothermal tuning cycle. As P_{inc} is increased, α first decreases at an almost constant rate until around $P_{inc} = 6.7$ mW where α decreases sharply due to the absorption resonance. For P_{inc} values between 7 and 10 mW, α once more decreases at an almost constant rate. As P_{inc} is decreased from 10 mW, α increases at an almost constant rate until $P_{inc} = 0.7$ mW where α suddenly increases. The lower plateau observed between $P_{inc} = 0.7$ and 7 mW in the photothermal tuning cycle gives the self-stable operation points that correspond to the TE_{35}^{1} WGM absorption. Self-stable operation points are located on the increasing half (region with positive slope) of a specific peak in the $\tilde{Q}_{abs}$ function, as shown with the red box in the inset of Fig. 1b. Around such a self-stable operation point, an increase or decrease in size is followed by an increase or decrease in $\tilde{Q}_{abs}$, respectively. These tend to bring the system back to the initial operating point, ensuring the self-stable operation. In contrast, self-stable operation is not observed around points located on the decreasing half (region with negative slope) of a peak in the $\tilde{Q}_{abs}$ function, as shown with the blue circle in the inset of Fig. 1b. Around such a point, an increase or decrease in size is followed by a decrease or increase in $\tilde{Q}_{abs}$, respectively. Hence the system quickly goes away from such an operation point.

III. Surface preparation and experimental setup

Experiments are performed on Rhodamine B-doped micrometer-sized NaCl–water droplets standing on a superhydrophobic surface, and kept in a sealed humidity chamber. The surface is placed at the focus of a microscope objective which enables visual selection of the studied microdroplet. The same microscope objective is used for focusing various lasers onto the microdroplet and collecting the fluorescence. Fluorescence from the Rhodamine B dye in the microdroplets is analyzed by a spectrometer.

The superhydrophobic surface is prepared by spin coating 50 mg/mL ethanol dispersions of hydrophobically-coated

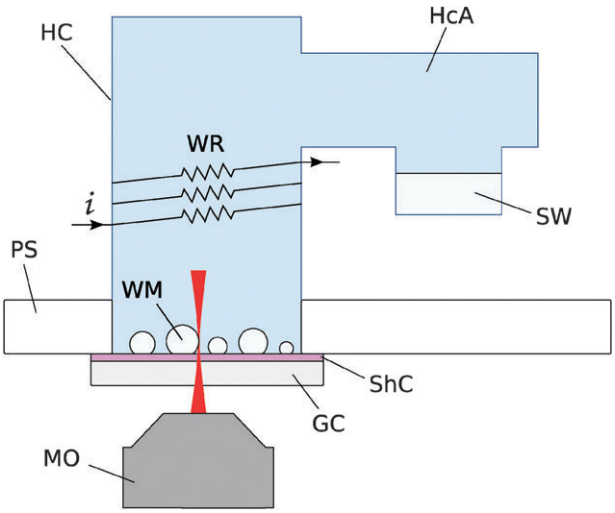

Fig. 2 Sealed chamber containing the microdroplets (lateral cut). HC: humidity chamber. WM: water microdroplet. ShC: superhydrophobic coating. GC: glass cover. SW: salt water reservoir. HcA: humidity-controlled atmosphere. PS: plexiglass support. MO: microscope objective. WR: wire resistor.

silica nanoparticles (Evonik, Aeroxide® LE2) on cover glasses. For millimeter-sized droplets, the average contact angle was reported to be larger than 150° for these surfaces.[22] NaCl–water microdroplets are sprayed on the superhydrophobic surface with an ultrasonic nebulizer at room temperature and pressure, using a water solution containing 2.85 M of dissolved NaCl and 10 μM Rhodamine B. The surface containing the microdroplets is then attached to the bottom of the humidity chamber. Optical experiments are performed after the microdroplets reach their equilibrium sizes (equilibrium NaCl concentration 3.83 M for $S_A = 0.8434$) within several hours.

The humidity chamber is depicted in Fig. 2. The main chamber body is made of glass; a small extension on one side is filled with a water solution saturated with KCl, enabling a high and stable relative humidity of 0.8434 in the whole chamber. The glass body is glued onto a plexiglass support with a hole allowing immersion of the microdroplets into the chamber's atmosphere by attaching the nanoparticle-coated cover glass to the bottom of the plexiglass support, thus sealing the chamber hermetically. The wire resistor depicted in the figure enables controlled heating of the chamber and the enclosed air. When required by the experiment, for example to provide a temperature perturbation to test the spectral stability of the microdroplets, a current is sent through the wire resistor for a given amount of time. We also plan to use this device as an actuator for active temperature stabilization in the future.

The optical setup is sketched in Fig. 3. A CW infrared laser ($\lambda = 1064$ nm, maximum output power = 300 mW) is used for controllable local heating of the microdroplets. The laser is linearly polarized at its output. A computer-controlled step motor adjusts the rotation of a half-waveplate, followed by a polarizing cube beam splitter. The undeflected output of the cube is sent to the experiment, and the optical power at the deflected output is measured by a photodetector. At the beginning of each data acquisition, a quick calibration is performed by measuring the power at the photodetector for

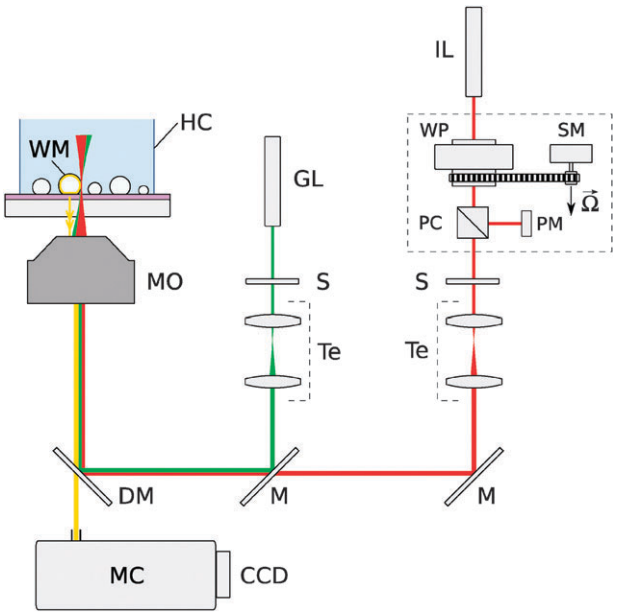

Fig. 3 Optical setup. From lasers to sample; IL: infrared laser. WP: ball bearing-mounted waveplate. SM: step motor. PC: polarizing cube. PM: powermeter. GL: green laser. S: electromechanical shutter. Te: telesope. M: mirror. DM: dichroic mirror. MO: microscope objective. HC: humidity chamber (partially drawn). WM: water microdroplet. DM: dichroic mirror. MC: monochromator. CCD: charge coupled device camera.

different waveplate angles, also providing a measurement of the total available power in the process. This setup enables precise tuning of infrared laser power in a reproducible manner, immune to long term fluctuations of the power at the output of the laser. A mechanical shutter is placed on the path of the infrared laser beam after the beamsplitter for rapid switching without the need to rotate the motor. A CW green laser (λ = 532 nm) is used to probe the fluorescence of the Rhodamine B dye in the microdroplets. A mechanical shutter is placed on its path to enable dye excitation only for the duration of the exposure of the spectrometer to fluorescence light. Respectively, green and infrared laser excitation powers of 1–10 μW and 0–10 mW at the focus of the microscope objective are typically used in the experiments.

Both laser beams are combined with a beam splitter and enter through the input port of an inverted microscope. Inside the microscope, the beam is reflected off a dichroic mirror and focused with the high numerical aperture microscope objective (NA = 1.4, 60× oil) in the inverted geometry. The combined beam is focused to the rim of the microdroplet being studied, which is selected out of several resting on the super-hydrophobic surface attached to the humidity chamber. Fluorescence from the Rhodamine B molecules is collected using the same objective and recorded with a spectrometer composed of a 50 cm monochromator and a CCD camera (spectral resolution of 0.15 nm around 590 nm). A 500 ms exposure time is used in all the spectra reported in this article. A readout time of ~1.5 s follows each exposure of the CCD sensor. Power-normalized emission spectra are used to generate all the contour plots shown in this article.

IV. Results and discussion

A Experimental hysteresis curves

Fig. 4b shows the change in the spectral position of a WGM of a 14 μm diameter NaCl–water microdroplet as a function of the incident infrared laser power (P_{inc}) during two consecutive photothermal tuning cycles. The specific WGM that was selected is indicated as WGM A in Fig. 4a. During each photothermal tuning cycle, P_{inc} is first increased from its minimal value and then decreased back to its starting point. In both cycles, a horizontal plateau is observed where the spectral position of the WGM remains almost stable at around 583.1 nm while P_{inc} is decreased from its maximum value. This position corresponds to a self-stable operation point. The observed horizontal plateau of self-stable operation is much flatter in Fig. 4b than the one calculated in Fig. 1, indicating the high quality ($Q > 1000$) of the absorption resonance which gave rise to self-stable operation in the experiment. This is consistent with the large microdroplet diameter used in the experiment (14 μm) as compared to that assumed in the calculations (~10 μm).[23] In Fig. 4b, a small offset is observed between the consecutive hysteresis curves as P_{inc} is increased, due to slight fluctuations in the ambient atmosphere. Such an offset is not observed at the spectral position of the self-stable

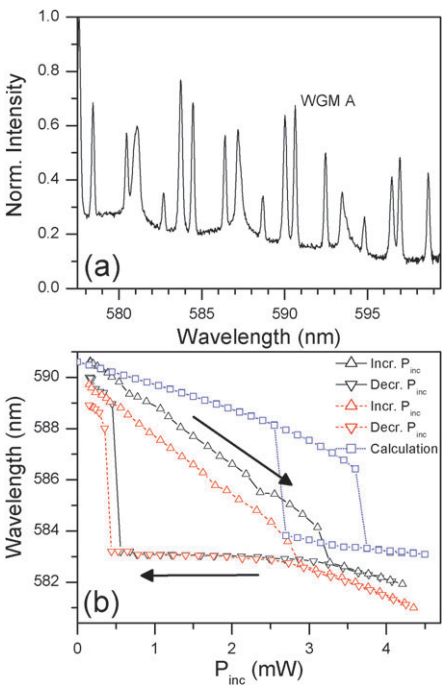

Fig. 4 (a) Normalized emission spectrum recorded from a 14 μm diameter NaCl–water microdroplet. (b) Triangles show the hysteresis curves obtained by plotting the change in the spectral position of WGM A during two consecutive photothermal tuning cycles. The horizontal plateau observed at 583.1 nm as P_{inc} is decreased corresponds to the self-stable operation point in both hysteresis curves. Fluctuations in the ambient atmosphere lead to a drift between the consecutive hysteresis curves. No drift is observed at the self-stable point. Squares show the calculated hysteresis in the spectral drift of the TM^{1}_{89} WGM. The horizontal plateau at 583.9 nm shows self-stabilization due to the absorption of the 1064 nm laser by the TE^{1}_{47} WGM.

point. This is due to the fact that the specific WGM absorption resonance that gives rise to stable operation is mainly determined by the refractive index of the microdroplet and this parameter remains almost constant between consecutive photothermal tuning cycles. Hence, the absence of the spectral drift is a clear indication of self-stable operation in that spectral position. We note that as P_{inc} is decreased, a sudden spectral jump of approximately 0.1 nm is observed at around $P_{inc} = 0.78$ mW. This is attributed to the multiline spectrum of the diode-pumped solid state infrared laser used in the experiments.

By matching the experimentally observed family of WGMs that includes the WGM A to first order modes, the radius of the microdroplet is determined as $a = 6.6733$ μm, assuming the real part of the refractive index to be 1.3677 at around 590 nm.[19] By this method, the polarization and angular momentum number of the WGM A are estimated to be TM^{1}_{89}. A hysteresis curve computed considering the refractive index at 1064 nm ($n = 1.3544 + 1112.15 \times 10^{-9}i$) and $a = 6.6733$ μm is shown in Fig. 4b, assuming that the infrared laser is focused exactly at the rim of the microdroplet at $y = 6.6733$ μm with a focal waist of $w_0 = 1000$ nm. Self-stable operation due to the absorption of the infrared laser by the TE^{1}_{47} WGM is predicted with a horizontal plateau at around 583.9 nm. The spectral position of the plateau matches approximately with the experimentally observed one (583.1 nm). We attribute the slight difference between these two spectral positions mainly to the errors in radius determination by mode-matching and to those in the refractive indices assumed at ~590 and 1064 nm. Non-uniformities in the refractive index within the microdroplet could also play a role in the observed differences.[24] The calculations also differ from the experiments in the absolute infrared laser powers at which state sudden changes occur in the hysteresis curve. This is mainly attributed to different positions of the focal spot between the experiment and calculations, and to the assumptions used in the thermodynamical model.[6,7]

B Resilience to an external perturbation

Another proof of the self-stable operation is shown in Fig. 5 where 80 consecutive spectra recorded from an 18 μm diameter microdroplet at 2.5 s intervals are plotted in the presence (Fig. 5a) and absence (Fig. 5b) of self-stabilization. In both cases, the ambient atmosphere that is initially at rest is perturbed by heating the wire resistor surrounding the humidity chamber for 3 s at 4.25 W (indicated by dashed lines in the figure). In the presence of self-stabilization, no change is observed in the spectral position of the WGMs within the spectral resolution of the experimental setup following resistive heating. In contrast, in the absence of self-stabilization a considerable blue shift of 4.8 nm is observed after 65 spectra recorded following resistive heating.

Fig. 5c shows the calculations reproducing these experimental results. In this figure, we plot the calculated spectral drift of the WGMs at around 590 nm as S_A is gradually increased from 0.8434 to 0.8477 in the absence or presence of self-stabilization. S_A is changed at 5 s intervals following a

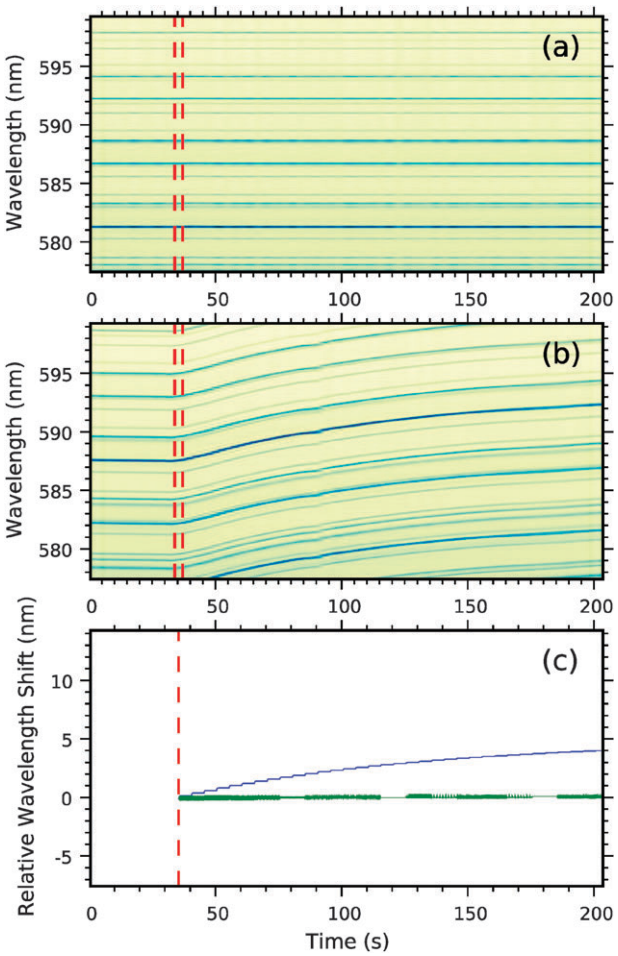

Fig. 5 Wavelength stability of a group of WGMs from an 18 μm diameter NaCl–water microplet undergoing an external heating perturbation, with accumulated spectra taken at 2.5 s intervals. (a) Microdroplet locked into self-stable operation. The effect of the perturbation (dashed lines) is barely seen. (b) Regular (unlocked) operation. The perturbation initiates a marked drift to the blue of the WGM wavelengths. (c) Calculations showing the spectral drift of the WGMs at around 590 nm as a result of gradual increase in S_A from 0.8434 to 0.8477 in the absence and presence of self-stabilization.

decaying exponential to match the shape of the experimentally observed spectral drift (Fig. 5b). In the absence of self-stabilization, the initial radius is selected to be $a = 5.0735$ μm (corresponding to $\alpha = 29.96$ at $\lambda = 1064$ nm), and the infrared laser power is assumed to be zero ($P_{inc} = 0$ mW). For the case of self-stabilization, the microdroplet is assumed to be initially locked at the operation point $P_{inc} = 5.67$ mW and $\alpha = 29.639$ in the hysteresis curve of Fig. 1b. All other parameter values for these calculations are assumed to be identical to those used for Fig. 1b. The calculated spectral drift is observed to follow the decaying exponential variation of S_A with a maximum spectral drift of ~4 nm within the time frame of the experiment in the unstabilized case, whereas for the stabilized case the drift is limited to ~0.2 nm. This matches quite well with the experimental results shown in Fig. 5a–b. In the stabilized case, the calculated spectral drift is slightly larger than the experimental value. This is mainly attributed to the relatively lower quality factor of the absorption resonances in the calculation due to

the smaller microdroplet size compared to the experiment ($a \sim 9$ μm).

C Long time self-stabilization

Fig. 6 shows the data recorded from a 14 μm diameter microdroplet that was self-stabilized for a long time. The hysteresis curve (Fig. 6a) shows two self-stable operation points around 585.4 and 590.3 nm. After recording the hysteresis curve, the microdroplet was self-stabilized at the first self-stable operation point (A, shown with the dashed line in Fig. 6a). Consecutive spectra were then recorded at a constant P_{inc} value of 2.02 mW (Fig. 6b), demonstrating that the locked operation could be maintained for up to one hour. During this period, no change was observed in the spectral position of the WGMs within the spectral resolution of the experimental setup (0.15 nm), corresponding to a radius stabilization within a few nanometers. The maximum duration for which we have been able to keep a microdroplet at a self-stable operation point was more than 1.5 h (data not shown). For comparison, consecutive spectra recorded from the same microdroplet in the absence of self-stabilization ($P_{inc} = 0$ mW, all other experimental conditions identical) are shown in Fig. 6c. In this case, the spectral position of the WGMs are observed to drift slowly due to fluctuations in the ambient atmosphere. The results from the locked microdroplet compare favorably with the previous self-stabilization demonstration relying on dye absorption.[11] The maximum stabilization time with that method was only a few minutes, limited by the change in dye absorption with photobleaching. As the method presented here relies solely on water absorption, photobleaching does not pose a fundamental limitation. No such limit now exists and locking could in theory be maintained for longer periods by keeping the chamber conditions stable over the long term using an external active temperature stabilization system.

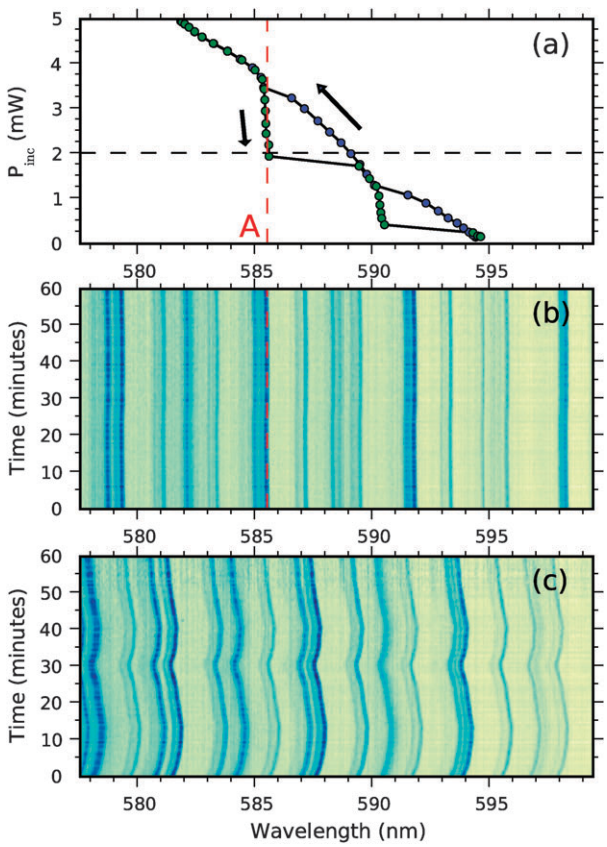

Fig. 6 Long time stability of WGMs from a 14 μm diameter microdroplet. (a) Hysteresis curve obtained by following a WGM in the emission spectra recorded from the microdroplet, in which two self-stable operation points exist. Blue and green circles indicate increasing and decreasing P_{inc}, respectively. (b) Time-accumulated spectra for the microdroplet locked at $P_{inc} = 2.02$ mW (dashed red line). No spectrum change is observed for an hour. (c) Time-accumulated spectra for the same microdroplet, unlocked ($P_{inc} = 0$ mW). The WGMs drift slowly. The number of spectra in (a) and (b) is 112.

D Optical bistability

Bistable operation is revealed from the hysteresis curves obtained during photothermal tuning of microdroplets. In a typical hysteresis curve, there exists a large region where a given infrared laser power corresponds to two spectral positions and, hence, two microdroplet sizes (see Fig. 4). Among the two spectral positions, the one that lies at the smaller wavelength (position A in Fig. 7a) belongs to the locked part of the curve where self-stability is observed and for which the microdroplet becomes immune to the fluctuations in the ambient

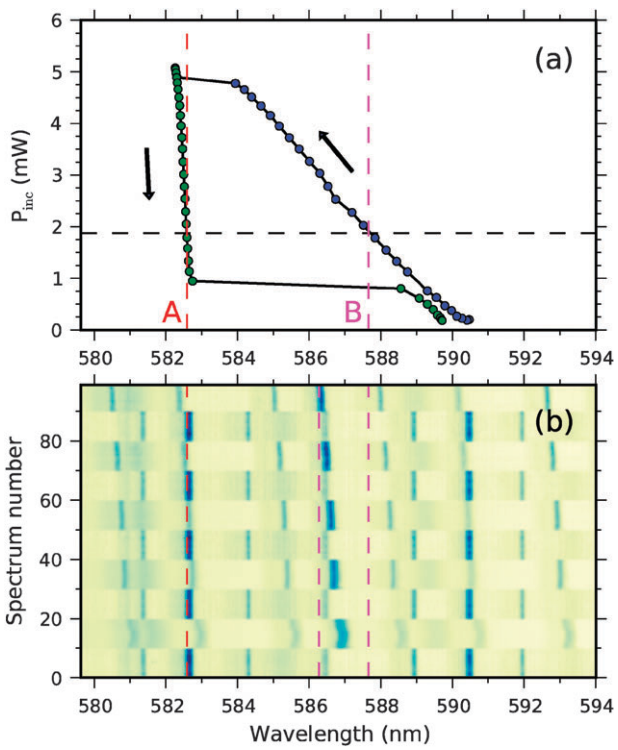

Fig. 7 Optical bistability observed from a 12 μm diameter microdroplet. (a) Hysteresis curve obtained by following a WGM in the emission spectra recorded from the microdroplet. Blue and green circles indicate increasing and decreasing P_{inc}, respectively. (b) Time-accumulated spectra for the same microdroplet exhibiting bistable behavior, recorded at $P_{inc} = 1.87$ mW. The delay between consecutive spectra for a given state (A or B) is 2.5 s. Additional delay when switching between states is 1 s from A to B, and 8 s from B to A.

atmosphere, to a large extent. The second spectral position lies at a larger wavelength, on the unlocked part of the curve (position B in Fig. 7a). It is possible to switch almost reversibly between these two spectral positions using a simple experimental procedure. While in the locked state (A), switching to the unlocked state (B) is realized simply by blocking the infrared laser for $\sim$500 ms and unblocking it. It is then possible to switch back from state B to state A by following the right-hand part of the hysteresis curve (path indicated by the arrows in Fig. 7a), *i.e.* by smoothly increasing and decreasing again the infrared laser power. Fig. 7b shows series of accumulated spectra with repeated switchings between states A and B, demonstrating that the system indeed exhibits the characteristics of optical bistability. State A is stable at all times, which is the signature of the self-stable operation point, as explained in section 4.1. In contrast, state B slowly drifts towards smaller wavelengths due to fluctuations in the ambient atmosphere. In Fig. 7b the dashed vertical lines indicate the spectral position of the state A (red color) and the range of spectral positions of the state B (purple color). After 9 switching events, the two states are still very much distinguishable despite the spectral drift of state B by almost 1.5 nm. The spectral drift observed in state B may be prevented by a conventionnal temperature stabilization feedback circuit using a Peltier element and a temperature sensor. In this way, the wavelength of state (B) would be kept within a reasonable range so that it could always be clearly distinguishable from that of state (A).

V. Conclusions

In conclusion, a self-stabilization mechanism has been demonstrated for NaCl–water microdroplets that makes their volume and WGM spectrum resilient to environmental perturbations (Fig. 5). Computations, using a rate equation-based thermodynamic model, and experiments confirmed the explanation of the mechanism by the presence of WGM absorption resonances when scanning the power of an infrared laser focused at the rim of a microdroplet. The rate of change of the microdroplet volume is very different when increasing or decreasing the power, *i.e.* a hysteretic behavior is observed (Fig. 1, 4, 6 and 7), if the infrared laser becomes resonant with a WGM absorption within the photothermal tuning cycle. Self-stable equilibrium is observed on one side of the hysteresis loops, when the power is decreased. The self-stabilization mechanism enables a locking of the microdroplet size and spectrum for hours (Fig. 6), as it relies only on photothermal effects inherent to the water microdroplet and independent of dye photobleaching, unlike the locking effect demonstrated in our previous work.[11] Spectral positions of the WGMs were self-stabilized within the experimental resolution (0.15 nm) for several hours, corresponding to a radius stabilization of only a few nanometers. The WGM spectrum was also switched reversibly (Fig. 7) between the locked and unlocked states by using the bistable nature of the system, effectively functioning as an optical memory device. For future experiments, an active temperature stabilization system that will keep the conditions in the humidity chamber stable can be used in order to increase the maximum time of size locking and improve the reversibility while switching between the bistable operation points.

The demonstrated self-stabilization technique enables characterization and exploitation of the ultrahigh quality WGMs of liquid microdroplets under stable experimental conditions, and using them to build stable sensors and light sources. Such devices could also make use of multiple microdroplets all locked at the same size. Coupled resonator optical waveguide (CROW) structures[25] built using exactly size-matched microdroplets can be readily envisioned. Optical bistability in a photothermal tuning cycle may also be used in designing novel optical devices such as a microdroplet-based optical memory device.

The authors thank the Alexander von Humboldt Foundation for equipment donation. A. Kiraz acknowledges the financial support of TÜBA in the framework of the Young Scientist Award program (Grant No. A.K/TÜBA-GEBIP/2006-19). M. Mestre acknowledges partial supports from TÜBİTAK and Koç University postdoctoral fellowship program.

References

1 T. Carmon, L. Yang and K. J. Vahala, *Opt. Express*, 2004, **12**, 4742.
2 M. H. Fields, J. Popp and R. K. Chang, in *Progress in Optics*, ed. E. Wolf, Elsevier, 2000, vol. 41, pp. 1–95.
3 J. P. Reid, H. Meresman, L. Mitchem and R. Symes, *Int. Rev. Phys. Chem.*, 2007, **26**, 139.
4 A. Kiraz, A. Kurt, M. A. Dündar and A. L. Demirel, *Appl. Phys. Lett.*, 2006, **89**, 081118.
5 A. Kiraz, Y. Karadağ and A. F. Coskun, *Appl. Phys. Lett.*, 2008, **92**, 191104.
6 A. Kiraz, Y. Karadağ and M. Muradoğlu, *Phys. Chem. Chem. Phys.*, 2008, **10**, 6446.
7 A. Kiraz, Y. Karadag, S. C. Yorulmaz and M. Muradoglu, *Phys. Chem. Chem. Phys.*, 2009, **11**, 2597.
8 E. Abraham and S. D. Smith, *Rep. Prog. Phys.*, 1982, **45**, 815.
9 S. Arnold, K. M. Leung and A. Pluchino, *Opt. Lett.*, 1986, **11**, 800.
10 S. Arnold, T. R. O'Keeffe, K. M. Leung, L. M. Folan, T. Scalese and A. Pluchino, *Appl. Opt.*, 1990, **29**, 3473.
11 A. Kiraz, A. Kurt, M. A. Dündar, M. Y. Yüce and A. L. Demirel, *J. Opt. Soc. Am. B*, 2007, **24**, 1824.
12 R. G. Picknett and R. J. Bexon, *J. Colloid Interface Sci.*, 1977, **79**, 667.
13 G. McHale, S. Aqil, N. J. Shirtcliffe, M. I. Newton and H. Y. Erbil, *Langmuir*, 2005, **21**, 11053.
14 I. N. Tang, A. C. Tridico and K. H. Fung, *J. Geophys. Res.*, 1997, **102**, 23269.
15 http://www.engineeringtoolbox.com/.
16 J. A. Lock and G. Gouesbet, *J. Opt. Soc. Am. A*, 1994, **11**, 2503.
17 G. Gouesbet and J. A. Lock, *J. Opt. Soc. Am. A*, 1994, **11**, 2516.
18 J. A. Lock, *Appl. Opt.*, 1995, **34**, 559.
19 D. R. Lide, *CRC Handbook of Chemistry and Physics Internet Version 2005*, http://www.hbcnetbase.com, CRC Press, 2005.
20 D. Segelstein, Master's thesis, University of Missouri, Kansas City, 1981.
21 E. J. G. Peterman, F. Gittes and C. F. Schmidt, *Biophys. J.*, 2003, **84**, 1308.
22 M. Y. Yüce, A. L. Demirel and F. Menzel, *Langmuir*, 2005, **21**, 5073.
23 A. Serpengüzel, J. C. Swindal, R. K. Chang and W. P. Acker, *Appl. Opt.*, 1992, **31**, 3543.
24 A. K. Ray, V. Devarakondab and Z. Gaoa, *Faraday Discuss.*, 2008, **137**, 85.
25 B. M. Möller, U. Woggon and M. V. Artemyev, *Opt. Lett.*, 2005, **30**, 2116.